Najafi Amin
Seif Mohammad Saeed

http://dx.doi.org/10.21278/brod67103

ISSN 0007-215X
eISSN 1845-5859

RANS SIMULATION OF HYDROFOIL EFFECTS ON HYDRODYNAMIC COEFFICIENTS OF A PLANING CATAMARAN

UDC 629.5.022.22:629.572:629.5.017.2:519.6:629.5.015.2
Original scientific paper

Summary

Determination of high-speed crafts' hydrodynamic coefficients will help to analyze the dynamics of these kinds of vessels and the factors affecting their dynamic stabilities. Also, it can be useful and effective in controlling the vessel instabilities. The main purpose of this study is to determine the coefficients of longitudinal motions of a planing catamaran with and without a hydrofoil using RANS method to evaluate the foil effects on them. Determination of hydrodynamic coefficients by experimental approach is costly, and requires meticulous laboratory equipment; therefore, utilizing numerical methods and developing a virtual laboratory seems highly efficient. In the present study, the numerical results for hydrodynamic coefficients of a high-speed craft are verified against Troesch's (1992) experimental results. In the following, after determination of hydrodynamic coefficients of a planing catamaran with and without foil, the foil effects on its hydrodynamic coefficients are evaluated. The results indicate that most of the coefficients are frequency independent especially at high frequencies.

Key words: *Hydrodynamic Coefficients; Catamaran; foil; Computational Fluid Dynamics, (CFD)*

1. Introduction

A planing vessel is a high-speed vessel with beam-based Froude number greater than 1.0 [1]. While many advances have been achieved in the seakeeping analysis of small displacement vessels, there has been little progress in the field of high-speed vessels due to their complicated hydrodynamic operation. Study of high-speed vessels hydrodynamics and their performance review, has led to the study of dynamics of such vessels. In this regard, determination of the hydrodynamic coefficients for dynamic equations for these vessels is necessary. Unfortunately, despite normal vessels, these coefficients are nonlinear functions of the motion and speed of the planing vessel. Dynamics of high-speed vessels have been studied by a few researchers. However, there are large differences in the methods applied by different authors.

Since Ursell, who first used a method of series expansion by wave free potentials (Ursell, 1949), different theories were developed to calculate the added mass and damping forces on

oscillating ship like sections, with the aim of predicting ship motions in waves [2]. The first experiments on oscillating sections were performed by Tasai (Tasai, 1960) [3] and Porter (Porter, 1960) [4] and later on by Paulling and Richardson (Paulling and Richardson, 1962) [5]. The first experimental studies on the hydrodynamics of multi-hull vessels can be traced to Everest (1968) and also, Turner and Taplin (1968). Since then, several researchers have performed theoretical, numerical and experimental studies on fast vessels in calm water conditions. From 1969 to 1971, Fridsma carried out vast experiments on a series of vessels with constant deadrise in regular and irregular waves [6, 7]. Ogilvie and Shen in 1973 studied the dynamic stability of a two-dimensional planing plate. These researchers supposed the problem to be a 2D problem where the only degree of freedom was wetted surface changes [8]. De Zwaan carried out the forced oscillation tests on a planing vessel in various velocities in 1973 [9]. In 1978, Martin developed a mathematical model based on strip theory to study porpoising stability and coupled linearized heave, pitch and surge motions [10, 11]. Payne in 1990, using his experience in the field of high-speed vessels, developed planing vessel motion simulator software in order to determine the hydrodynamic coefficients based on 2D strip theory [12].

Today, investigation of high-speed vessels seakeeping is a combination of experimental, analytical and numerical methods. In 1992, Armin Troesch determined the hydrodynamic coefficients by experimental method. Troesch indicated that the wetted surface and hydrodynamic coefficients of a planing vessel are time-dependent and frequency-dependent, respectively [1]. Insel and Molland (1992) highlighted, experimentally and numerically, some hydrodynamic features of catamarans; they focused on the effects on the overall resistance performance as a result of varying the main demi-hull dimension and separation length [13]. In 1994, Grigoropoulos used the results obtained by towing tank tests and carried out a numerical and experimental study on the effects of transient and regular waves on recreational vessels [14]. Klaka and McCook in 1999 performed an experimental study on heave and pitch motions of a vessel [15]. Varyani et al. (2000) [16] have presented the behavior of a catamaran hull form with and without forward speed. Like the previous authors, two different methods have been used, namely, strip theory and the three-dimensional pulsating-source method. There were negligible differences at zero forward speed in both methods.

Recent researches to predict the motions of vessels are based on numerical methods with viscous flow assumption. The numerical methods based on Reynolds Averaged Navier-Stokes (RANS) equations, are one of the most reliable numerical methods to predict the motions of the vessels. In this method, the Navier-Stokes equations along with a turbulence model are solved in a computational grid. A large number of these RANS simulations are carried out for roll motion. 3D examples of roll motion simulation are provided in by Chen et al. 2001 [17] as well as Miller et al. 2002 [18]. However, the 6 degree of freedom (6 DOF) simulations to investigate the full set of motions is required. In this regard, the simulation of vertical motion of the vessel is the first step. There are some recent studies on three-dimensional vessel vertical motions by Sato et al. 1999 [19] who provided results for Wigley and series 60 vessels. Paterson et al. (2003) provided a RANS-based software called “CFDSHIP-IOWA”, which is an evolved version of previous researchers’ works such as Wilson, Stern and Rhee (1998-2002) [20, 21, and 22]. Lugni et al. (2004) emphasized on the role of the nonlinear effects for extreme sea conditions, which has motivated the present research work. The use of RANS-based solvers for analysis of seakeeping of catamarans is rather rare. The geometry chosen for their study is the Delft 372 catamaran, which is a typical high-speed multi-hull model [23]. Weymouth et al. (2005) simulated heave and pitch motions of Wigley vessel by RANS method. Their numerical simulation results indicated a good agreement with experimental results [24]. Souto-Iglesias et al. (2007) analyzed the interference resistance of multi-hulls by assessing its relationship with the shape and amplitude of the wave train between the hulls for a specific planing vessel design. The free model condition was then considered, making it more difficult to identify interference

effects due to substantially different dynamic trims and sinkages between the mono-hull and the catamaran [25]. Larsson et al. (2010) simulated the motions of KCS2 and KVLCC2 tanker in head sea condition using RANS equations [26]. Broglia et al. (2011) and Zaghi et al. (2011) used a CFD solver to simulate multi-hulls instead, and found a good agreement for the resistance values describing complex interference effects at high Froude number regimes [27]. The RANS method was used by Sadat Hosseini (2013) in order to study roll motion and the parameters influencing it [28].

Considering the preamble mentioned above, the hydrodynamic coefficients of high-speed vessels can be derived by using numerical methods based on RANS equations. The utilized method in order to determine the hydrodynamic coefficients, is based on Troesch's 1992 and Journee's 1992 method [29]. To validate the proposed method in this study, the motions of the high-speed mono-hull vessel used by Troesch 1992, were simulated. The determined hydrodynamic coefficients obtained by this method indicated a good agreement with Troesch's experimental results. Next, the same procedure was used to evaluate the hydrodynamic coefficients for a high-speed catamaran equipped with a foil, and the effects of changes in velocity and frequency were investigated. It should be noted that using foils on aircraft wings and rockets, in order to control the lift force and height, has been successfully implemented. The initial idea of using foils on high-speed vessels is based on this success. The vessels using waterjet propulsion system may suffer from low stability due to the lack of draft levels. This lack of stability can be compensated by installing active and passive control systems. However, due to the drag force and the lack of space for conventional systems, the designers took advantage of using foils (see Fig. 1).

Fig. 1 Foil between catamaran hulls

Karafiath and Fisher indicated that using the similar elements can increase the trim motion range from 0.4 to 2.0 degrees and cause 2% reduction in fuel consumption of the design speed [30]. The results of the experiments indicate that reduction in resistance leads to reduction in fuel consumption and emissions, and therefore an increase in speed. Tsai and Hwang indicated that interceptors can reduce trim in motion and planing vessels resistance effectively [31]. Recent experimental works carried out in this area are based on utilizing a combination of interceptor and foil, simultaneously. In the present study, attempt has been made to determine the ideal angle of the foil and ideal length of interceptor when they are simultaneously used. One of the latest studies on interceptor and foil effects on high-speed vessels was presented in 2009 by Steen [32].

2. Problem definition

Consider a high-speed vessel with a right-handed coordinate system as shown in Fig. 2. Heave motion (vertical displacement of the center of gravity) and Pitch motion (rotation about the Y axis) are shown in this figure. Using Newton's second law, the 2 DOF equations of heave and pitch motions around the center of gravity are as follows:

$$\left(\rho\nabla + A_{33}\right).\ddot{Z} + B_{33}.\dot{Z} + C_{33}.Z + A_{35}.\ddot{\theta} + B_{35}\dot{\theta} + C_{53}.\theta = X_{w3} \quad (1)$$

$$\left(I_{yy} + A_{55}\right).\ddot{\theta} + B_{55}.\dot{\theta} + C_{55}.\theta + A_{53}.\ddot{Z} + B_{53}.\dot{Z} + C_{53}.Z = X_{w5} \quad (2)$$

Where Z and θ are the heave and pitch motions, respectively (see Fig. 2).

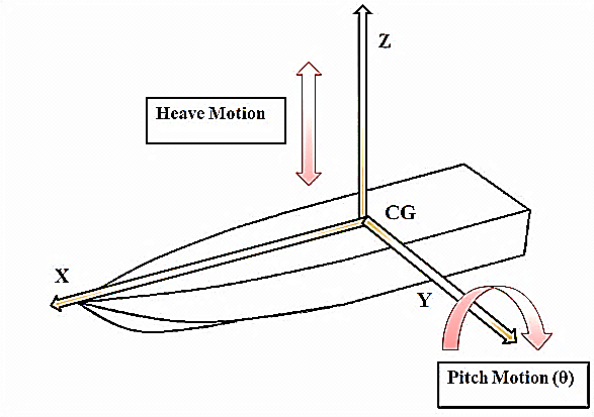

Fig. 2 Heave and pitch directions (z *and* θ)

The hydrodynamic coefficients A_{ij} (added mass hydrodynamic coefficient) and B_{ij} (damping hydrodynamic coefficient) are determined by model tests, commonly (Journee 1992 and Troesch 1992) [1, 29]. In these tests, the vessel is forced to have pure heave and pitch in constant speed. Then, the forces, moments, and the phase lag between the motions and measured forces are determined and then the hydrodynamic coefficients will be determined by using some relevant relations. In experimental tests, the forces and moments acting on vessel are provided by electrical or mechanical motors and the model is towed in a towing tank. Fig. 3 shows a simple schematic of this test. If the vertical rods move perfectly harmonic ($S1 = S2$), the vessel will experience a forced heave motion. And similarly, for forced pitch motion, two rods are under vertical oscillatory motions in the opposite direction relative to each other.

In the following, the method of determination of hydrodynamic coefficients using forced heave and pitch motions will be explained.

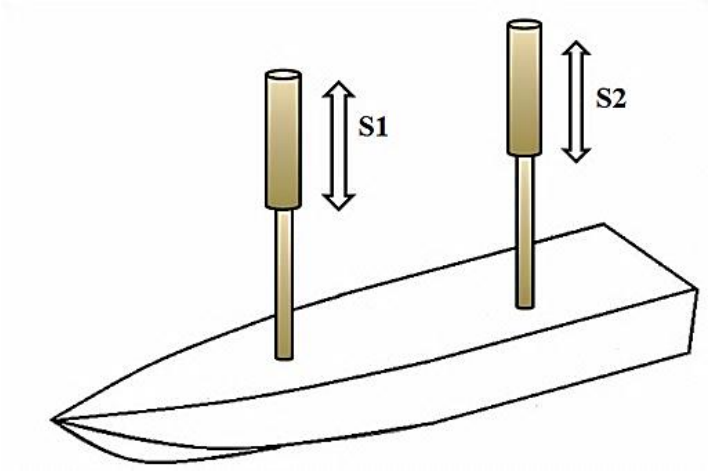

Fig. 3 Forced heave and pitch for a high-speed vessel

2.1. Forced harmonic heave motion

When the vessel is under forced heave motion, the equations of motion can be written as follows:

$$Z = Z_a.cos(\omega t) \tag{3}$$

$$(M_{33} + A_{33}).\ddot{Z} + B_{33}.\dot{Z} + C_{33}.Z = X_{03a}.\cos\left(\omega t + \varepsilon_{X_{03z}}\right) \tag{4}$$

$$A_{53}.\ddot{Z} + B_{53}.\dot{Z} + C_{53}.Z = X_{05a}.\cos\left(\omega t + \varepsilon_{X_{05z}}\right) \tag{5}$$

Fig. 4 shows a vessel under forced heave motion. Z_a and ω are the motion amplitude and frequency, respectively.

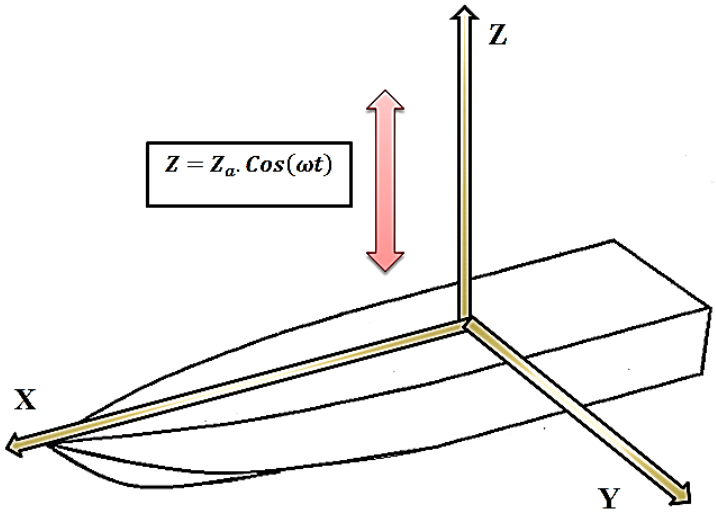

Fig. 4 A vessel under forced heave motion

Equation (5) expresses the forced heave motion with known motion amplitude and frequency. In order to derive the coefficients, every Z variable and its derivatives in equations (4) and (5), will be substituted by equation (3). Therefore the right side of equations (4) and (5) can be expanded:

$$-(M_{33} + A_{33}).Z_a\omega^2 cos(\omega t) - B_{33}.Z_a\omega sin(\omega t) + C_{33}.Z_a cos(\omega t) = \tag{6}$$
$$X_{03a}.\cos(\omega t)cos\left(\varepsilon_{X_{03z}}\right) - X_{03a}sin(\omega t)\,sin(\varepsilon_{X_{03z}})$$

$$-(A_{53}).Z_a\omega^2 cos(\omega t) - B_{53}.Z_a\omega sin(\omega t) + C_{53}.Z_a cos(\omega t) \tag{7}$$
$$= X_{05a}.\cos(\omega t)cos\left(\varepsilon_{X_{05z}}\right) - X_{05a}sin(\omega t)\,sin\left(\varepsilon_{X_{05z}}\right)$$

By setting equality between coefficients of $sin(\omega t)$ and $cos(\omega t)$ in both sides of equations, the hydrodynamic coefficients of forced heave motion will be derived as follows:

$$A_{33} = -\frac{X_{03a}.\cos\left(\varepsilon_{X_{03z}}\right)}{Z_a.\omega^2} + \frac{C_{33}}{\omega^2} - M_{33} \tag{8}$$

$$B_{33} = +\frac{X_{03a}\sin\left(\varepsilon_{X_{03z}}\right)}{Z_a.\omega} \tag{9}$$

$$A_{53} = -\frac{X_{05a}.\cos\left(\varepsilon_{X_{05z}}\right)}{Z_a.\omega^2} + \frac{C_{53}}{\omega^2} \tag{10}$$

$$B_{53} = +\frac{X_{05a}\sin\left(\varepsilon_{X_{05z}}\right)}{Z_a.\omega} \tag{11}$$

$$C_{33} = +2\rho g\int_0^L y_w.dx_b \tag{12}$$

$$C_{53} = -2\rho g\int_0^L y_w.x_b.dx_b \tag{13}$$

Where:

x_b is the longitudinal position of cross sections of the vessel.

y_w is half-breath of the water plan of the vessel.

2.2. Forced harmonic pitch motion

When the vessel is under forced pitch motion, the equations of motion can be written as follows:

$$\theta = \theta_a.cos\left(\omega t\right) \tag{14}$$

$$\left(M_{55} + A_{55}\right).\ddot{\theta} + B_{55}.\dot{\theta} + C_{55}.\theta = X_{05a}.\cos\left(\omega t + \varepsilon_{X_{05\theta}}\right) \tag{15}$$

$$A_{53}.\ddot{\theta} + B_{53}.\dot{\theta} + C_{53}.\theta = X_{03a}.\cos\left(\omega t + \varepsilon_{X_{03\theta}}\right) \tag{16}$$

Fig. 5 shows a vessel under forced pitch motion. θ_a and ω are the motion amplitude and frequency, respectively.

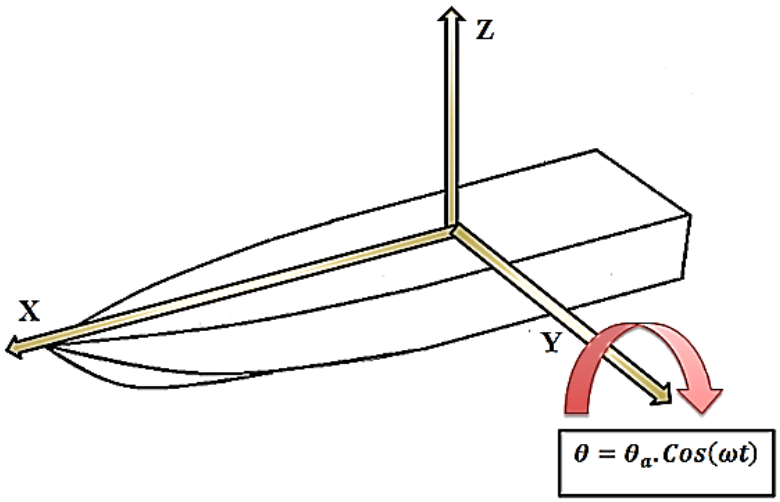

Fig. 5 A vessel under forced pitch motion

Similar to forced harmonic heave motion, with substituting θ and its derivatives in equations (15) and (16) from equation (14) and setting the equality of the coefficients of $cos(\omega t)$ and $sin(\omega t)$, the hydrodynamic coefficients of forced pitch motion will be derived as follows:

$$A_{55} = -\frac{X_{05a}.\cos\left(\varepsilon_{X_{05z}}\right)}{\theta_a.\omega^2} + \frac{C_{55}}{\omega^2} - M_{55} \tag{17}$$

$$B_{55} = +\frac{X_{05a}\sin\left(\varepsilon_{X_{05z}}\right)}{\theta_a.\omega} \tag{18}$$

$$A_{35} = -\frac{X_{03a}.\cos\left(\varepsilon_{X_{03z}}\right)}{\theta_a.\omega^2} + \frac{C_{35}}{\omega^2} \tag{19}$$

$$B_{35} = +\frac{X_{03a}\sin\left(\varepsilon_{X_{03z}}\right)}{\theta_a.\omega} \tag{20}$$

$$C_{55} = +2\rho g\int_0^L y_w.x_b.x_b.dx_b \tag{21}$$

$$C_{35} = -2\rho g\int_0^L y_w.x_b.dx_b \tag{22}$$

Where:

x_b is the longitudinal position of cross sections of the vessel.

y_w is half-breath of the water plan of the vessel.

Determination of hydrodynamic coefficients will depend on the force amplitude, harmonic moments and the phase lag between them and harmonic motions of the vessel. Troesch 1992 and Journee 1992 utilized model test and experimental facilities in order to determine the force and moments exerted to the vessel as well as the phase lag between them and vessel harmonic motions. For instance, Mr. Troesch used a planar Vertical Motion Mechanism (VMM) equipped with separate force, moment and motion sensors. This mechanism was installed and calibrated at University of Michigan in 1989. Using model test for forced harmonic heave and pitch in order to determine hydrodynamic coefficients is quite expensive. Besides the costs of model fabrication and experiments, these tests require a meticulous and complex mechanism for forced heave and pitch motions as well as accurate sensors in order to record forces, moments and motions, during the time that vessel is towed at a specific speed. On the other hand, the model fabrication and the mechanism calibration process make the tests very time-consuming. Therefore, it appears that creating a virtual numerical laboratory to determine these coefficients by numerical methods can be useful in understanding the hydrodynamics of high-speed vessels. In this virtual lab, the forces and moments as well as phase lags can be calculated accurately under forced heave and pitch motions. As previously mentioned, in this method the RANS equations are solved together with continuity equation for an incompressible fluid. In the following, after validating the numerical analysis results of mono-hull vessel with experimental results provided by Troesch 1992, the effect of the foil on hydrodynamic coefficients of a high-speed catamaran will be investigated.

3. Problem-solving method

The governing equation for conservation of mass in a compressible fluid flow can be written:

$$\frac{\partial \rho}{\partial t}+\frac{\partial}{\partial x_i}\left(\rho u_i\right)=0 \tag{23}$$

where ρ is the fluid density and u_i is the velocity component in each of the principal directions x, y and z. In addition, momentum conservation equation can be written as:

$$\frac{\partial}{\partial t}\left(u_i\right)+\frac{\partial}{\partial x_j}\left(u_i u_j\right)=\frac{1}{\rho}\left(-\frac{\partial P}{\partial x_i}+\frac{\partial \tau_{ij}}{\partial x_j}+\rho g_i+F_i\right) \tag{24}$$

where F_i and g_i represent body forces and gravitational acceleration, respectively. In this problem, the buoyancy and gravity are significant due to free surface effects. τ_{ij} is the Reynolds stress tensor which is defined as:

$$\tau_{ij}=\mu\left(\frac{\partial u_i}{\partial x_j}+\frac{\partial u_j}{\partial x_i}\right)-\frac{2}{3}\mu\frac{\partial u_i}{\partial x_i}\delta_{ij} \tag{25}$$

where δ_{ij} is the Kronecker delta, which is unity when i and j are equal and zero otherwise. Considering Equations (23)–(25), the Reynolds averaged momentum equation is derived as:

$$\frac{\partial}{\partial t}\left(u_i\right)+\frac{\partial}{\partial x_j}\left(u_i u_j\right)=\frac{1}{\rho}\left(-\frac{\partial P}{\partial x_i}+\frac{\partial}{\partial x_j}\left[\mu\left(\frac{\partial u_i}{\partial x_j}+\frac{\partial u_j}{\partial x_i}\right)-\frac{2}{3}\mu\frac{\partial u_i}{\partial x_i}\right]+\frac{\partial\left(\overline{u_i' u_j'}\right)}{\partial x_j}+\rho g_i\right) \tag{26}$$

In Eq. (26) $\overline{u_i' u_j'}$ is related to turbulence Therefore, a turbulence model is required. For turbulence description, the $k-\omega$ based Shear Stress Transport (SST) model with automatic wall functions (mixed formulation) which developed by Menter in 2003 [33] was employed where k and ω represent turbulence kinetic energy and turbulence specific dissipation rate, respectively. The SST model combines $k-\omega$ and $k-\varepsilon$ models with a blending function which changes the model from $k-\omega$ to $k-\varepsilon$ when the distance from the wall rises. Therefore, this model uses the good convergence rate of $k-\varepsilon$ high-Reynolds model and good accuracy of $k-\omega$ model, near the wall. This two-equation model, is the most appropriate turbulence model for predicting flow separation [33].

The "Volume of Fluid" (VOF) has been utilized for free surface modeling. This method assumes same pressure and velocity for all phases of a control volume and controls the fraction of phases. Thus, the governing equations will be solved for an equivalent single-phase fluid with physical characteristics as function of volume fraction for every control volume. For correct calculations near a wall, the near wall generated grid was based on no dimensional distance y^+. The y^+ values on the vessel surfaces for each case at all operating conditions were between 100 and 500 which allow the simulation of the flow in the proximity of the vessel surface with suitable accuracy together with using automatic wall function (considering the relatively high-Reynolds numbers of each case). For primary y^+ calculations, the Eq. (36) can be used on boundary layer on a flat plate:

$$\Delta y=L.y^{+}.\sqrt{74}.\left(Re\right)^{-\frac{13}{14}} \tag{36}$$

Where *L* is the characteristic length and *Re* is the flow's Reynolds number. Δy is the first node distance from the wall. The distances of the next nodes from the wall are increased by a growth rate (increasing factor) equal to 1.15 (-). y^+ is defined as:

$$y^+ = \frac{u_\tau \rho}{\mu} \Delta y \tag{37}$$

where Δy, ρ, μ are the normal distance from the wall, fluid density and viscosity, respectively, and u_τ is the friction velocity defined as:

$$u_\tau = \left(\frac{\tau_w}{\rho} \right)^{0.5} \tag{38}$$

Where, τ_w and u_τ are wall shear stress and shear velocity respectively.

4. Simulation of mono-hull vessel motions

In this section, the harmonic motions of a mono-hull vessel in calm water will be simulated based on RANS equations. Finally, the results of hydrodynamic coefficients will be validated with Troesch's [1] test results.

4.1. Geometrical characteristics and meshing

Air and water velocities were set 2.56 $\frac{m}{s}$ at inlet boundary equivalent to beam-based Froude number 1.5 (-). The vessel has an initial trim of 4 degrees (Troesch, 1992) [1]. Also, table 1 shows the actual vessel geometry for numerical modeling.

Table 1 Actual vessel geometry for numerical modeling

The monohull vessel geometrical characteristic	Unit	Value
Length	[m]	2.096
Width	[m]	0.318
Vertical center of gravity	[m]	0.195
Center of gravity	[m]	0.470
Wetted length-to-width ratio	[-]	3.00

A structured grid with approximately 710,000 elements was generated using ICEM CFD blocking method (Fig. 6). The dimensions of generated computational domain were $13m \times 3.0m \times 6.3m$. The mentioned dimensions were chosen considering far field location law. The numerical far field locations should be far enough from the vessel hull to avoid affecting the solution. The symmetry boundary condition was applied in order to reduce the number of elements and solution time. The dynamic mesh method has been used for this problem and the volumes and locations of the cells change by rigid body motions.

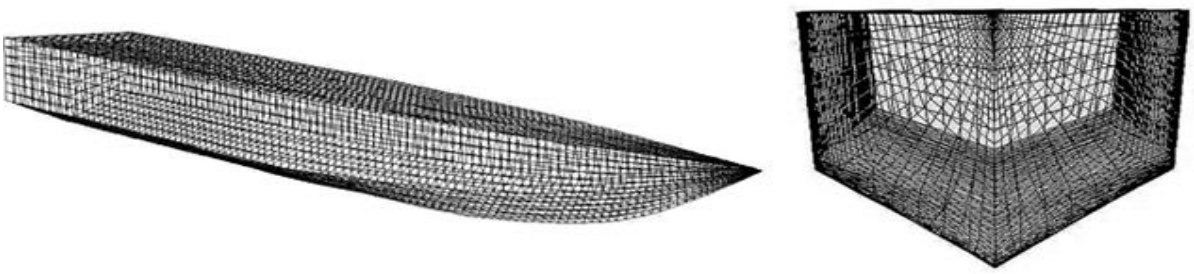

Fig. 6 Surface meshes of monohull high-speed vessel

4.2. Simulation results

As mentioned above, the purpose of using numerical methods is to determine the forces and moments on the vessel, the phase lag between them as well as the harmonic motions of the vessel. The hydrodynamic coefficients will be calculated through this process. For this purpose, the harmonic heave and pitch motions imposed on the vessel. Note that the motions amplitude and frequency have extracted from Troesch's experimental results (1992) [1]. These motions will be imposed to center of gravity. The numerical results are shown in Fig. 7. Results include harmonic forces and moments due to forced heave motion with amplitude of 2.54 cm and frequency of 4.72 (rad/sec), and forced pitch motion with amplitude of 0.026 radian and frequency of 4.72 (rad/sec).

4.2.1 Method of calculating the coefficients from the obtained results

As previously mentioned, determination of hydrodynamic coefficients of vessel, depend on force and moments amplitudes, the phase lag between them and the harmonic motion of the vessel. For this process, the time interval between the first harmonic heave and pitch motions trough, and the force and moments on the vessel are calculated. Subsequently, the phase lag between the harmonic and the force or moment will be determined by dividing this value by the period of the forced harmonic motion and multiplying the result by 360.

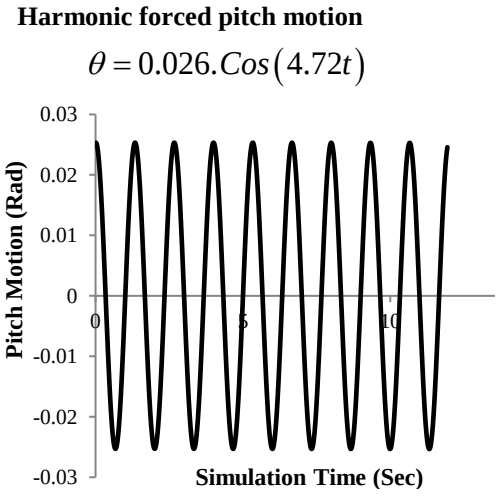

Harmonic pitch motion

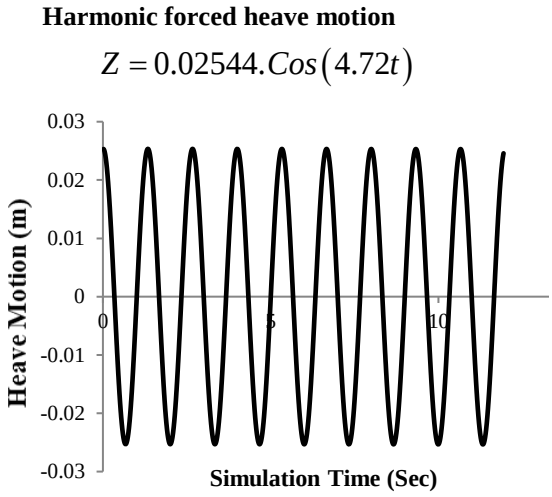

Harmonic heave motion

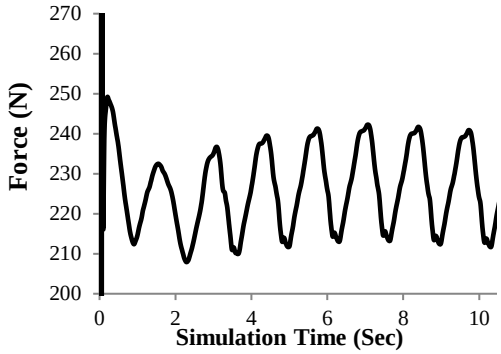

The changes of harmonic forces amplitude on vessel in harmonic pitch motion

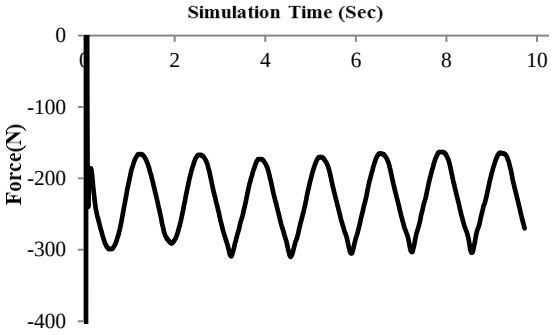

The changes of harmonic forces amplitude on vessel in harmonic heave motion

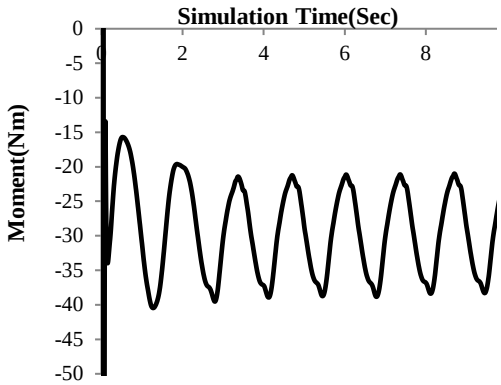

The changes of harmonic moments amplitude on vessel in harmonic pitch motion

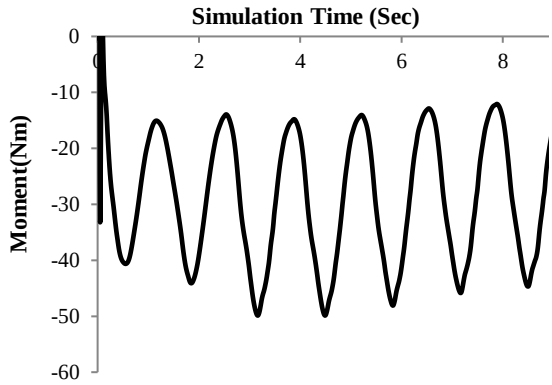

The changes of harmonic moment amplitude on vessel in harmonic heave motion

Fig. 7 Heave and pitch numerical results of monohull vessel

(As an example, the results of such analysis on the mono-hull vessel are shown in Fig. 7.). As indicated in Fig. 8, the time lag between the heave harmonic motion first trough and the force on the vessel (the value of 0.067 (s)) is divided by the period of harmonic heave motion (1.33 (s)) and then multiplied by 360. Therefore, the phase lag between harmonic force on vessel and the motion will be determined. Since the first trough of the wave occurs before the first trough of the harmonic motion, the phase lag between force and harmonic heave motion will be negative. The same methods were employed to determine all other phase lags. Fig. 8 shows the forces and moments as well as the phase lag between them and harmonic motions. In addition, the phase lag of force and moment amplitude will be determined. The values of force and moment amplitudes and phase lags are shown in Table 2 and 3.

Table 2 Forces, moments, and phase difference in forced harmonic heave motion

Harmonic force on vessel		Moment on vessel	
Amplitude	Phase difference	Amplitude	Phase difference
65.33 N	18.95 deg.	12.45 N.m	24.36 deg.

After determining the phase lags and amplitudes of the forces and moments, the stiffness factors of the vessel are required.

Table 3 Determination of Forces, moments, and phase difference in harmonic forced pitch motion

Harmonic force on vessel		Moment on vessel	
Amplitude	Phase difference	Amplitude	Phase difference
12.1 N	50.84 deg.	10.39 N.m	162.41 deg.

These factors depend on the geometry of the vessel body and are determined using the Simpson method. The stiffness factors for the high speed vessel under study are presented in Table 4.

Table 4 C static coefficient of high-speed vessel

Hydrostatic Coefficient	Value
C_{33} (N.m)	2975
C_{53} (N)	353
C_{35} (N)	353
C_{55} (N.m)	42

After determining the required parameters and putting them in the equations, the example of calculating the hydrodynamic coefficients is continued as follows:

$$A_{33} = -\frac{X_{03a}.\cos\left(\varepsilon_{X_{03z}}\right)}{Z_a.\omega^2} + \frac{C_{33}}{\omega^2} - M_{33} = 7.29$$

$$B_{33} = +\frac{X_{03a}\sin\left(\varepsilon_{X_{03z}}\right)}{Z_a.\omega} = 187.5$$

$$A_{53} = -\frac{X_{05a}.\cos\left(\varepsilon_{X_{05z}}\right)}{Z_a.\omega^2} + \frac{C_{53}}{\omega^2} = -4.17$$

$$B_{53} = +\frac{X_{05a}\sin\left(\varepsilon_{X_{05z}}\right)}{Z_a.\omega} = -42.27$$

$$A_{55} = -\frac{X_{05a}.\cos\left(\varepsilon_{X_{05z}}\right)}{\theta_a.\omega^2} + \frac{C_{55}}{\omega^2} - M_{55} = 3.41$$

$$B_{55} = +\frac{X_{05a}\sin\left(\varepsilon_{X_{05z}}\right)}{\theta_a.\omega} = 25.59$$

$$A_{35} = -\frac{X_{03a}.\cos\left(\varepsilon_{X_{03z}}\right)}{\theta_a.\omega^2} + \frac{C_{35}}{\omega^2} = 2.65$$

$$B_{35} = +\frac{X_{03a}\sin\left(\varepsilon_{X_{03z}}\right)}{\theta_a.\omega} = 76.45$$

Note that these coefficients are not dimensionless. The dimensionless coefficients are presented in Table 5.

Forced harmonic pitch motion

$$\theta = 0.026.Cos\left(4.72t\right)$$

Forced harmonic heave motion

$$Z = 0.02544.Cos\left(4.72t\right)$$

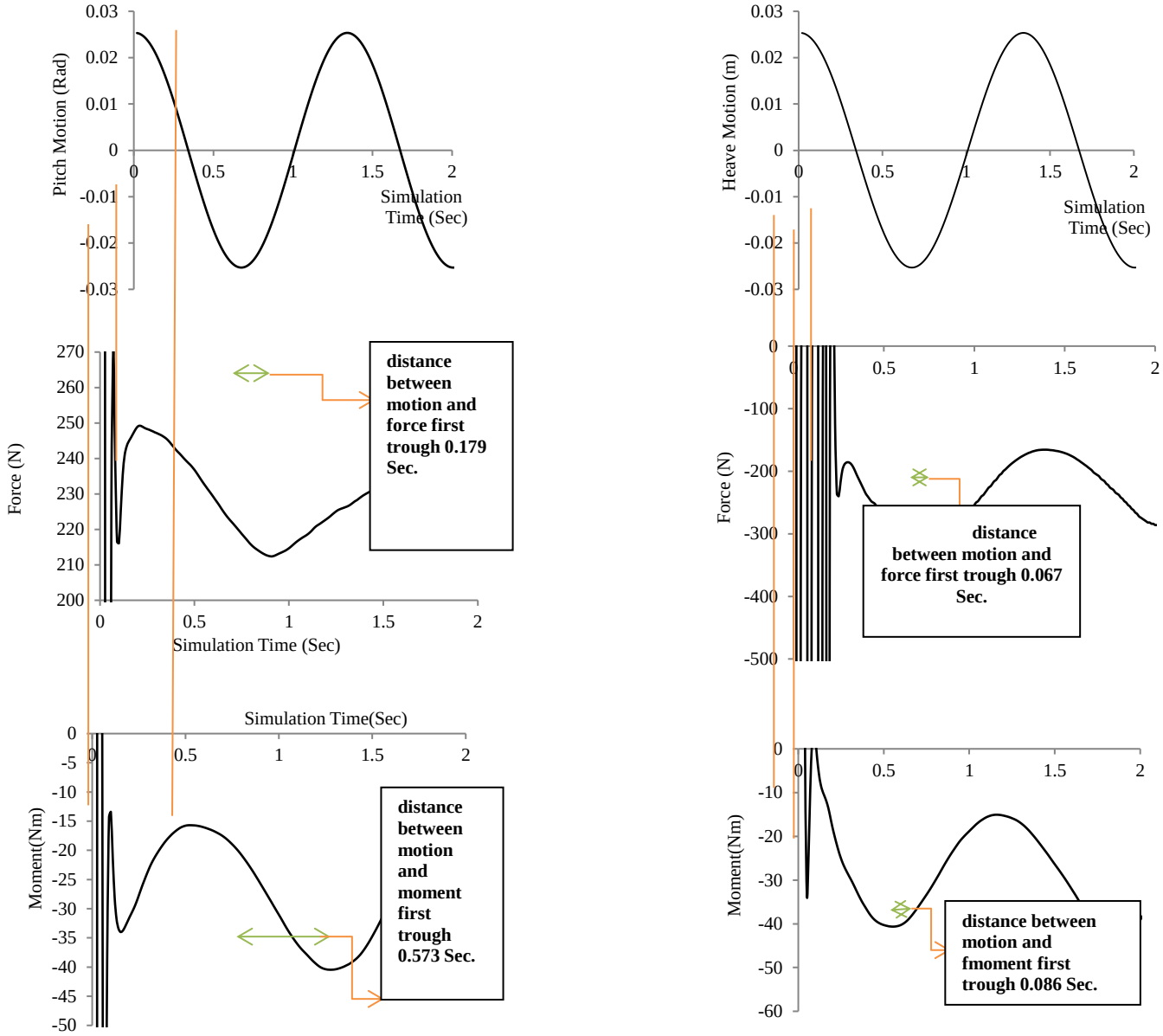

Fig. 8 Determination of phase difference between force and moment on vessel and harmonic motion

4.2.2 Validation

As mentioned previously, the Troesch's experimental results in 1992 [1] are used for validation. According to his test conditions, the beam-based Froude number was 1.50 (-) in the numerical simulation. There is a good agreement between the results of the numerical simulation in the current study and Troesch's experimental results (Fig. 9).

Table 5 Dimensionless hydrodynamic coefficients

$B_{53}^{"} = \frac{B_{53}}{\rho B^4 \sqrt{\frac{g}{B}}}$	$A_{55}^{"} = \frac{A_{55}}{\rho B^5}$
$A_{33}{}^{"} = \frac{A_{33}}{\rho B^3}$	$B_{55}^{"} = \frac{B_{55}}{\rho B^5 \sqrt{\frac{g}{B}}}$
$B_{33}^{"} = \frac{B_{33}}{\rho B^3 \sqrt{\frac{g}{B}}}$	$A_{35}^{"} = \frac{A_{35}}{\rho B^4}$
$A_{53}^{"} = \frac{A_{53}}{\rho B^4}$	$B_{35}^{"} = \frac{B_{35}}{\rho B^4 \sqrt{\frac{g}{B}}}$

In many cases, CFD simulations could not give quite accurate results. For instance, many parameters such as those of the turbulence models, boundary layer meshes, values of y^+, the size of computational domain and, etc., will affect the solution accuracy.

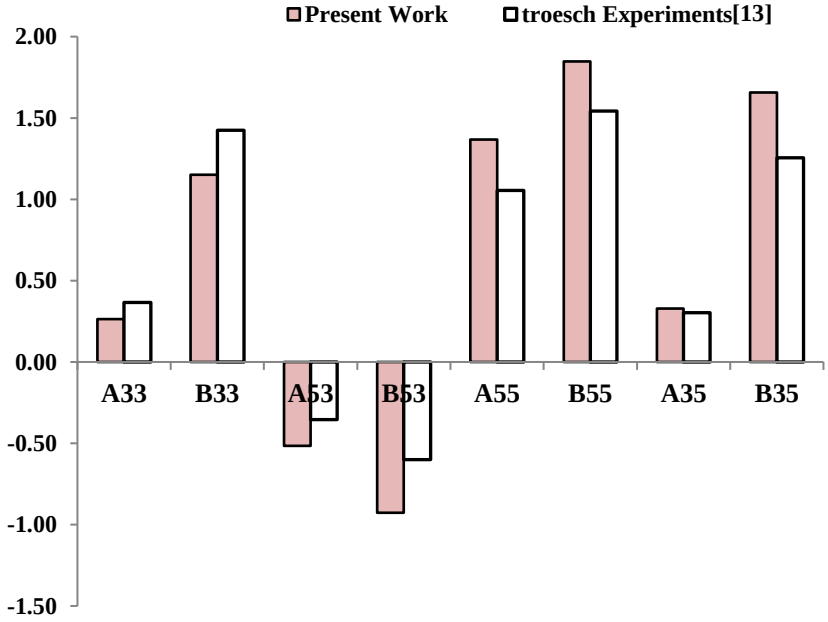

Fig. 9 Present numerical results vs. Troesch's experimental results

Considering this validation for mono-hull vessel, the same approach has been used to study the hydrodynamic coefficients of a high-speed catamaran to find out how these coefficients will change regarding the frequency alteration.

5. The catamaran geometrical characteristics and meshing

The dimensions of the catamaran vessel under study are shown in table 6. A structured grid with approximately 900,000 hexahedral elements is used as computational domain. The dimensions of the computational domain were 50(m)×72(m)×40(m). As mentioned before, in CFD simulations, the far field boundaries should be far away from the main body.

Table 6 Geometrical characteristics of the catamaran

Characteristic	Unit	Value
length	(m)	12.0
Width	(m)	3.4
Center of gravity	(m)	5.4

The geometry of this catamaran vessel is shown in Fig. 10. Similar to the mono-hull vessel case, the symmetry boundary condition was applied in order to reduce the number of elements and solution time.

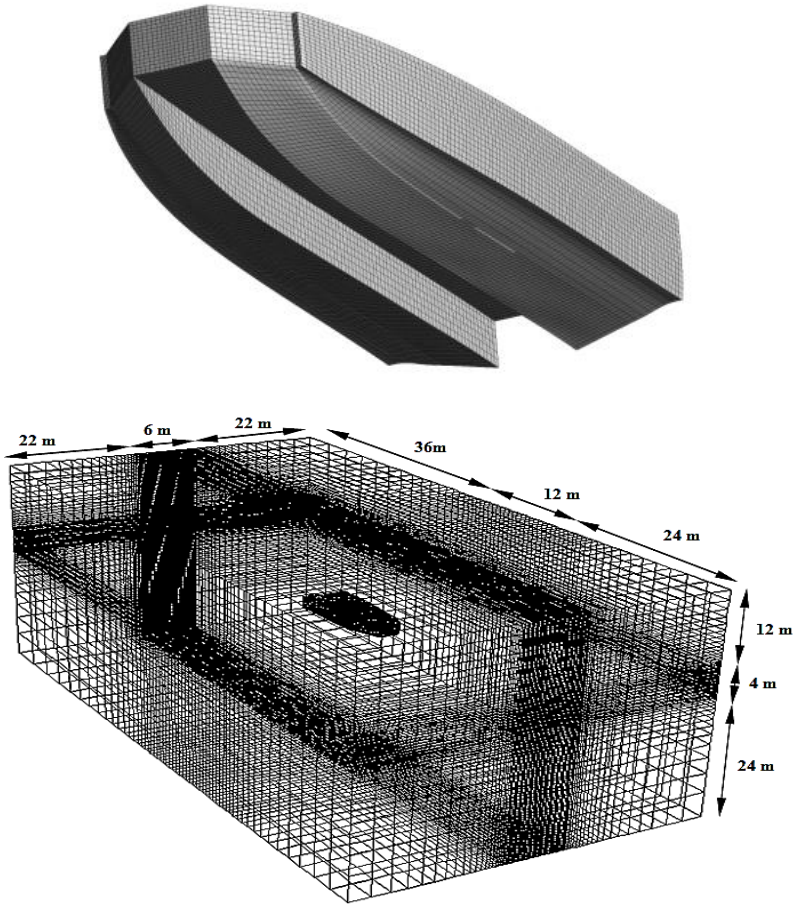

Fig. 10 Computational domain and its dimensions (down) and the body form and surface meshes (top)

Also, similarly, the dynamic mesh method employed for this problem. Therefore, volumes and locations of the cells will change by rigid body motions. The inlet velocity is 8.15 (m/s) which is equivalent to beam-based Froude number 1.2 (-). The initial conditions for this simulation were obtained after putting the vessel in hydrostatic conditions. After hydrostatic equilibrium, the draft and trim were obtained 0.6 (m) and 1.0 (deg), respectively. The surface meshes of this catamaran are shown in Fig. 10. By choosing the value of 300 for y^+, the thickness of the first layer was obtained to be approximately 1 (mm). The boundary layer was covered by at least ten layers of prismatic elements.

5.1. Simulation results

The results of forced heave and pitch motions respectively at frequency of 3.70 (rad/sec) and 2.59 (rad/sec), are shown in Fig. 11.

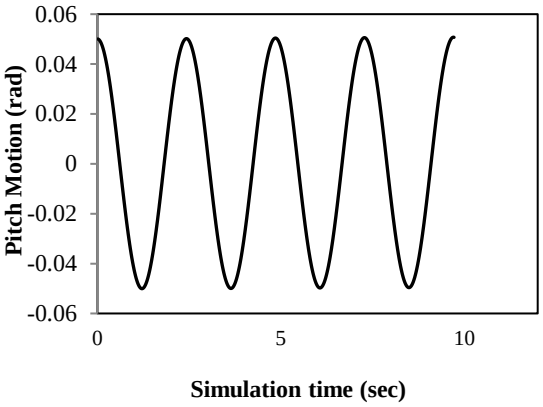

Pitch harmonic motion in frequency of 2.59 (rad/sec)

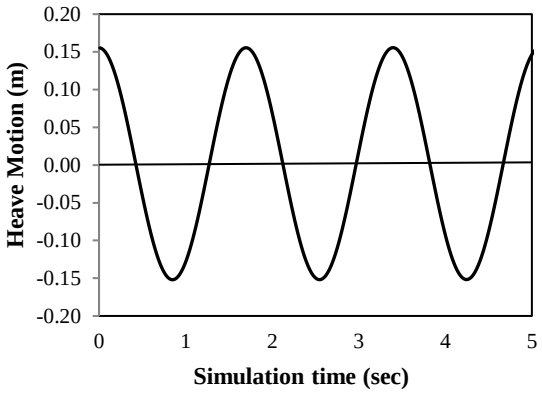

Heave harmonic motion in frequency of 3.70 (rad/sec)

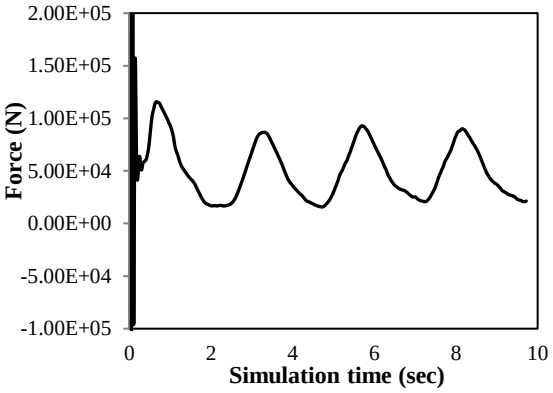

Harmonic forces changes on catamaran at frequency of 2.59 (rad/sec)

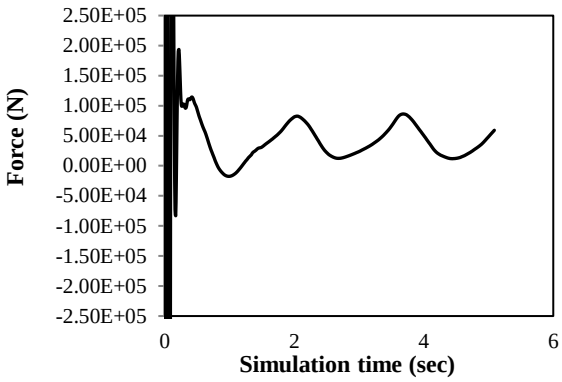

Harmonic forces changes on catamaran at frequency of 3.70 (rad/sec)

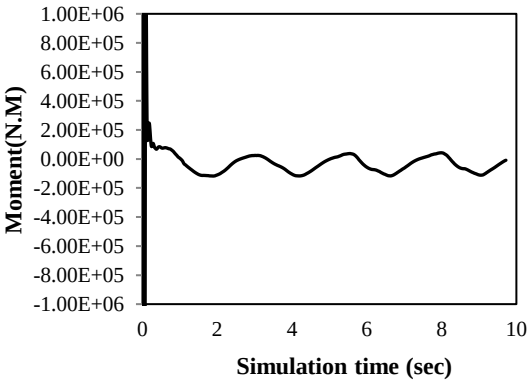

Harmonic moments changes on catamaran at frequency of 2.59 (rad/sec)

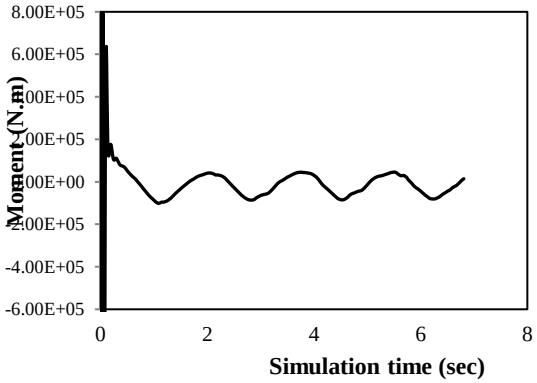

Harmonic moments changes on catamaran at frequency of 3.70 (rad/sec)

Fig. 11 Forces and moments on catamaran for forced heave motion in frequency of 3.7 (rad/sec) and forced pitch motion in frequency of 2.59 (rad/sec)

Note that the values of frequency and amplitude of the motion have been set based on the conditions in the Persian Gulf. In this case ω_e may be altered from 39.27 (rad/sec) to 2.59 (rad/sec). Also, at any ω_e the forces and moments on catamaran and their phase lag were recorded. The amplitude of forced heave and pitch motions were 16.0 (cm) and 0.052 (rad), respectively.

6. Adding foil to the catamaran

To study the effect of foil, the catamaran was equipped with foil at three locations: L/4, L/2 and 3L/4 respectively, where L is the length of vessel. The different locations of hydrofoil are shown in Fig. 12.

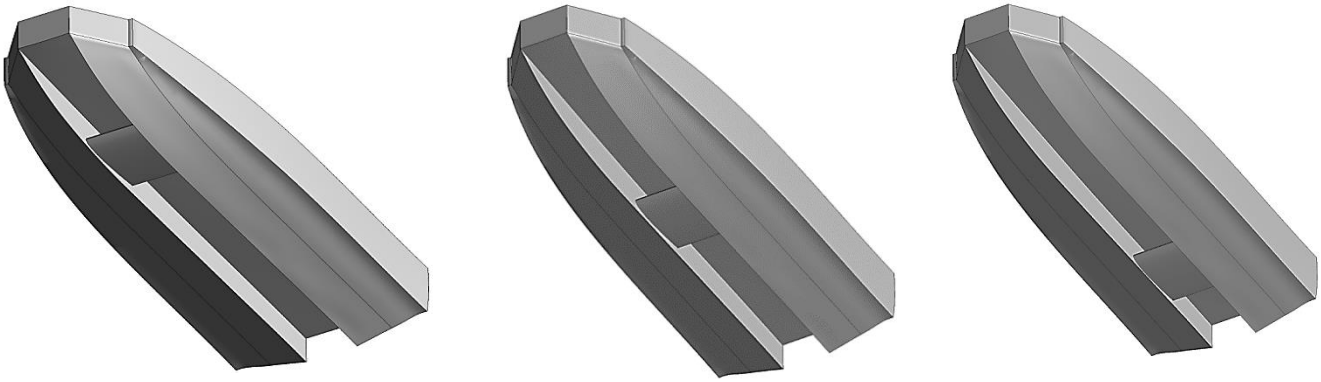

Fig. 12 Foil between catamaran demi-hulls

Results for the location L/4, in forced heave harmonic motion at frequency of 3.70 (rad/sec) and forced pitch harmonic motion at frequency of 2.59 (rad/sec) are shown in Fig. 13. It should be noted the values of motion frequency and amplitude were set according to the situations in the Persian Gulf as mentioned before.

6.1. The catamaran hydrodynamic coefficients with and without foil

In this section, the CFD simulation results of catamaran motions with and without foil will be presented. To determine the hydrodynamic coefficients of catamaran, the static coefficients C_{ij} should be determined at first. These coefficients depend on wetted area of the vessel and are determined using the Simpson method as previously mentioned. The stiffness factors of the high speed vessel geometry are presented in Table 7. Assuming small amplitude motions, the static coefficients C_{ij} can be assumed constant. Added mass and damping coefficients vs. frequency are shown in Figs. 14 and 15. In order to investigate the effects of added mass and damping to the vessel, a spring-damping-mass system has been used (see Fig. 16).

Table 7 C_{ij} static coefficients of catamaran

Static Coefficient	Value
C_{33} (N/m)	305311.71
C_{53} (N)	915935.13
C_{35} (N)	915935.13
C_{55} (Nm)	2747805.40

The motion of the mass under water causes its surrounding water to move. An amount of energy is created by the motion of the vessel and will recede by dispersive waves. Furthermore, some energy will be stored as the kinetic energy of the water particles as well as gravitational potential energy when the water particles move from the trough to the crest. The added mass is the difference between kinetic and potential energy [34]. For some special hulls and in some special frequencies, the added mass can be negative.

Forced pitch harmonic motion

$$\theta = 0.052.cos(\omega_e t)$$

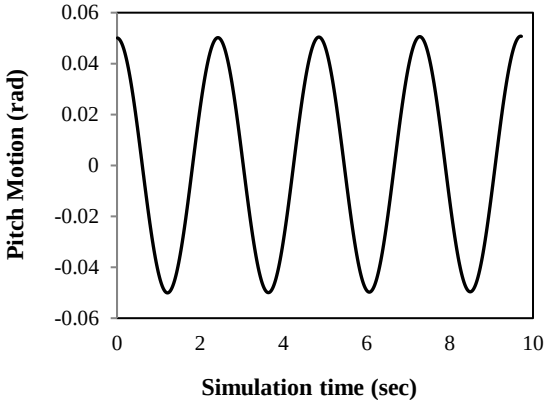

Harmonic pitch motion in frequency of 2.59 (rad/sec)

Forced heave harmonic motion

$$Z = 0.16.cos(\omega_e t)$$

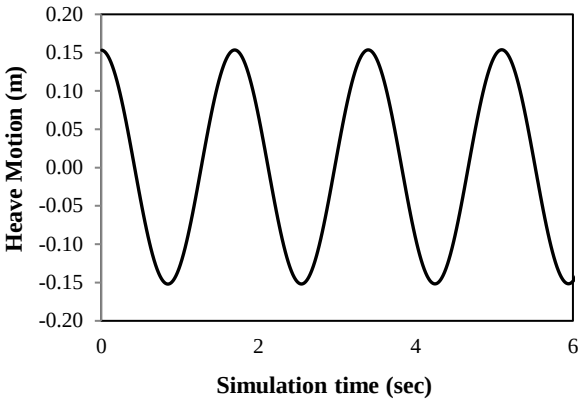

Harmonic heave motion in frequency of 3.70 (rad/sec)

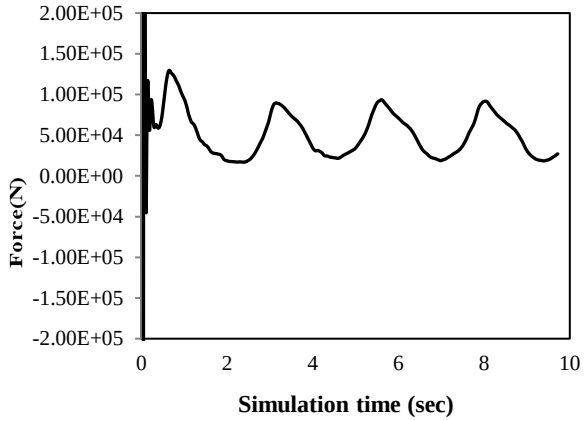

Harmonic forces changes on catamaran at frequency of 2.59 (rad/sec) with interceptor with the height of 7.0 (cm)

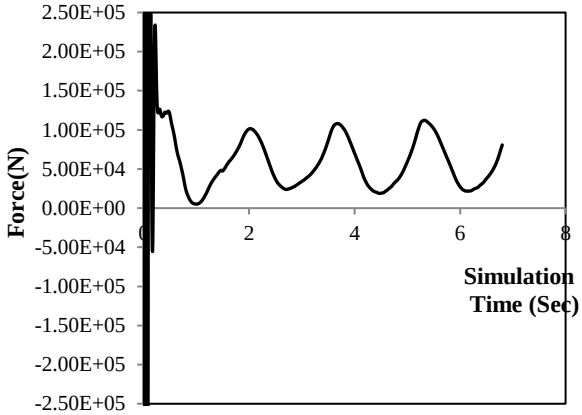

Harmonic forces changes on catamaran at frequency of 3.70 (rad/sec) with interceptor with the height of 7.0 (cm)

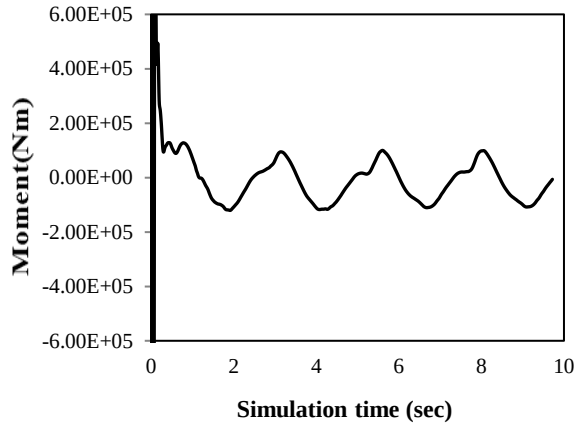

Harmonic moments changes on catamaran at frequency of 2.59 (rad/sec) with interceptor with the height of 7.0 (cm)

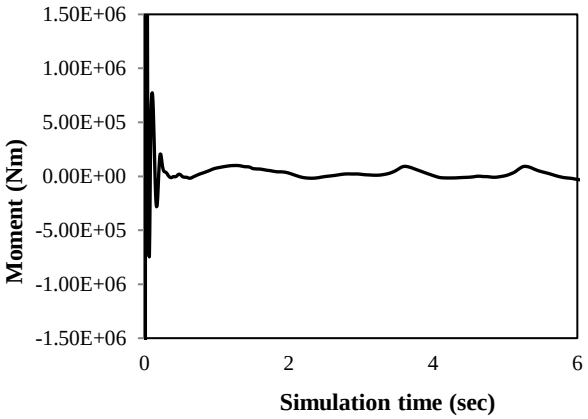

Harmonic moments changes on catamaran at frequency of 3.70 (rad/sec) with interceptor with the height of 7.0 (cm)

Fig. 13 Forces and moments on catamaran equipped with foil for forced heave motion in frequency of 3.7 (rad/sec) and forced pitch motion in frequency of 2.59 (rad/sec)

The negative added mass can occur for catamarans, blunt bodies and immersed bodies near the free surface. For instance, there is negative added mass for catamaran which is used in the present work. The negative added mass in pitch motion mode, occurred at the frequencies close to the lower frequency of the symmetric sloshing mode between two demi-bodies (ω_n). The same resonance in symmetric sloshing mode occurred for heave motion. Sloshing is resonant oscillations of water between two demi-bodies. The name "sloshing" was chosen because this phenomenon is similar to the sloshing in the tanks and in resonance frequency; the water trapped between two demi-bodies has a lot of turbulence. If the generated wave between two demi-bodies in pitch motion is of the full wavelength, the wave is symmetrical relative to the axis of symmetry of the vessel. The reason for this incident is the identical motions of two demi-bodies in heave motion. Therefore, a wave crest or trough will appear between the two demi-bodies. This is the reason that the first resonance between two demi-bodies in heave mode is named "symmetric sloshing mode".

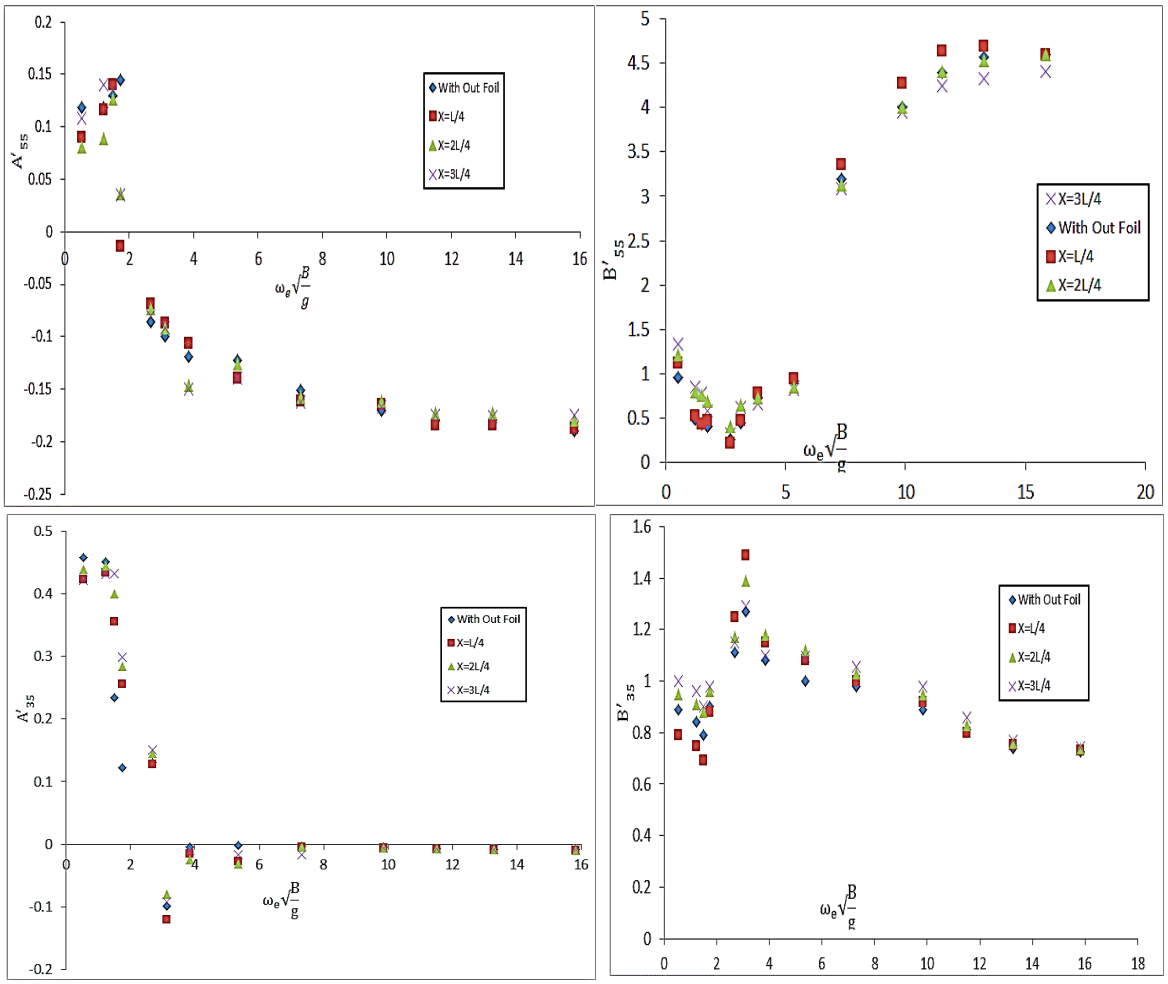

Fig. 14 Added mass and damping coefficients vs. frequency due to pitch motion

Assuming that resonance occurs when the distance between the two demi-bodies (separation distance) is equal to half the wavelength, the first resonance frequency is estimated as follows [34]:

$$\omega_n = \left(\frac{\pi g}{d}\right)^{0.5} \tag{47}$$

Where d and g are the distance between two demi-bodies and gravitational acceleration, respectively.

Considering the Eq. (47), it can be found out that by changing the distance between the two demi-bodies, the resonance occurrence will change. It should be noted that the Eq. (47) gives the first resonance frequency that is equal to the frequency of a wavelength equal to twice the distance between two demi-bodies. Since the generated standing waves will not give away any energy, the wave amplitude between the two demi-bodies is increased at sloshing resonance frequencies and there will be low damping at the space between the two demi-bodies. A feature of resonance systems with low damping is that when passing through the sloshing resonance frequency by changing excitation frequency, the phase will quickly change by 180 degrees. Therefore, the wave between two demi-bodies can be generated in-phase with heave and pitch accelerations and when passed through this frequency, there can be a 180 degree phase lag with the acceleration. This means that if the generated wave between two demi-body and acceleration of the heave and pitch motions are in-phase; the added mass will be positive because of the increment of acceleration.

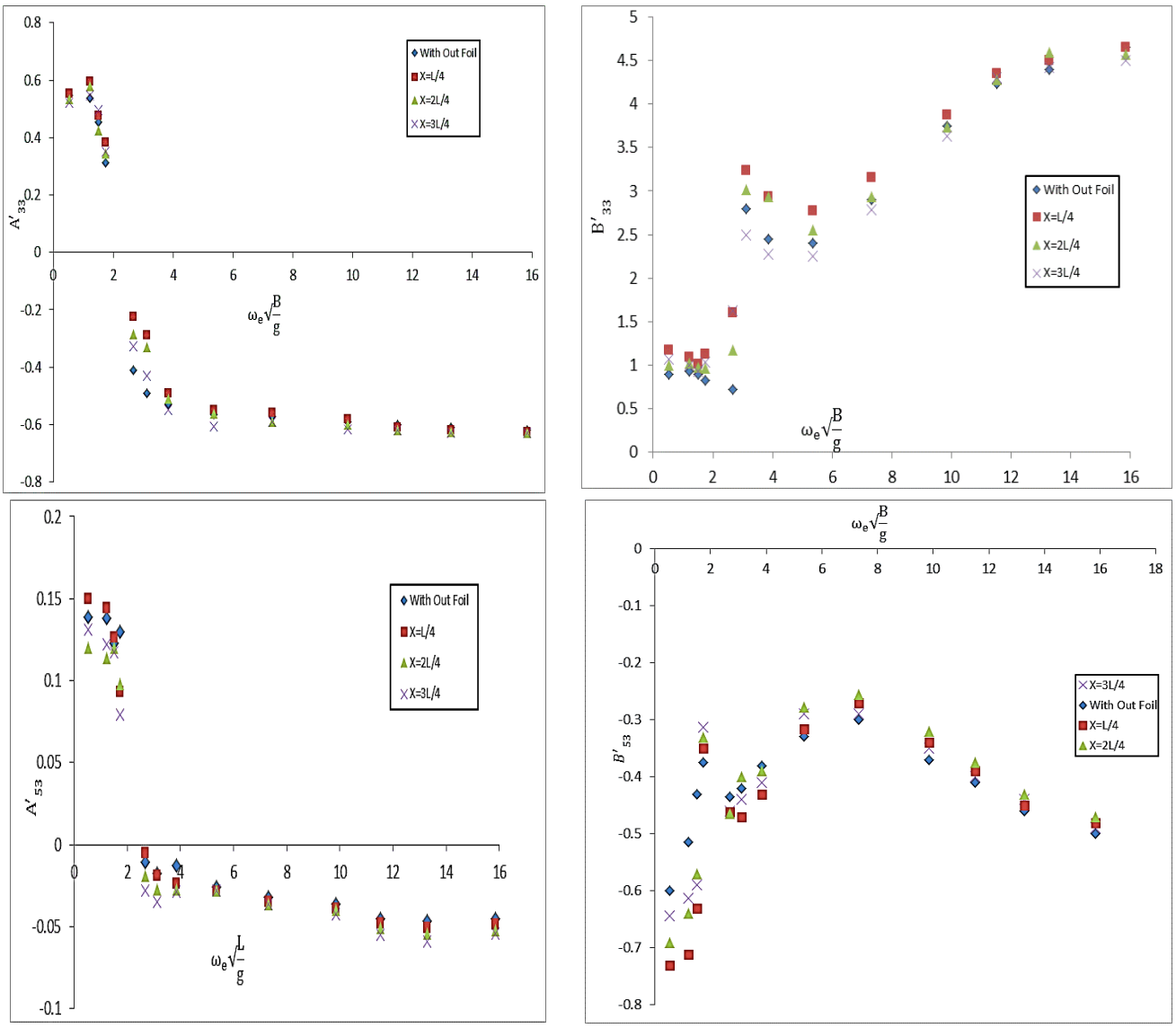

Fig. 15 Added mass and damping coefficients vs. frequency due to heave motion

Table 8. Added mass coefficient due to heave motion

$\omega_e\sqrt{\boldsymbol{B}}/\boldsymbol{g}$	A_{33}				Difference between coefficients values with and without foil		
	Without Foil	With foil					
		X=L/4	X=2L/4	X=3L/4	X=L/4	X=2L/4	X=3L/4
0.53	0.548	0.555	0.535	0.521	%1.28	%2.37	%4.93
1.21	0.537	0.596	0.578	0.546	%11	%7.64	%1.68
1.5	0.455	0.477	0.424	0.497	%4.84	%6.82	%9.23
1.73	0.314	0.383	0.345	0.35	%21.97	%9.87	%11.47
2.68	-0.41	-0.223	-0.285	-0.327	%45.61	%30.49	%20.24
3.11	-0.49	-0.29	-0.33	-0.43	%40.82	%32.66	%12.25
3.84	-0.53	-0.49	-0.51	-0.55	%7.55	%3.77	%3.77
5.36	-0.566	-0.55	-0.561	-0.607	%2.83	%0.88	%7.24
7.31	-0.57	-0.56	-0.59	-0.59	%1.75	%3.51	%3.51
9.85	-0.59	-0.58	-0.6	-0.615	%1.7	%1.7	%4.24
11.51	-0.6	-0.61	-0.62	-0.62	%1.67	%3.33	%3.34
13.28	-0.61	-0.62	-0.625	-0.628	%1.64	%2.46	%2.95
15.84	-0.62	-0.625	-0.63	-0.63	%0.81	%1.62	%1.61
18.41	-0.629	-0.628	-0.636	-0.628	%0.16	%1.11	%0.16

Vice versa, if the generated wave between two demi-body and acceleration of motions are out of phase; the added mass will be negative because of the decrement of acceleration. The hydrodynamic coefficients are shown in Figs. 14 and 15. Also, the values for A_{33} with and without foil are tabulated in table 8. According to the discussions above, it is expected that the hydrodynamic coefficients undergo an extreme with respect to frequency. Eq. (47) is used to determine the resonance frequency. Considering the separation distance (d) is equal to 1.2 m, the resonance frequency is determined as follows:

$$\omega_n = \left(\frac{\pi g}{d}\right)^{0.5} = \left(\frac{\pi g}{1.2}\right)^{0.5} = 5.06\left(rad/sec\right)$$

Therefore, in frequencies approximately equal to this resonance frequency, the added mass would take a negative value leading to an extreme point in the diagram of damping-frequency. This behavior is followed in Figs. 14 and 15. By increasing the frequency and passing through the resonance frequency, the diagrams of hydrodynamic coefficients at the high encounter frequencies tend to become constant. The dispersion relation for waves is as follows [35]:

$$\omega^2 = kg = \frac{2\pi}{\lambda} g \rightarrow \lambda = \frac{gT^2}{2\pi} \quad (48)$$

where λ and T are the wavelength and the wave period, respectively. The lack of change in hydrodynamic coefficients with respect to the frequency in high frequency values is shown in Figs. 14 and 15. It should be explained that by the encounter frequency increment, the encounter period is decreased, and considering the dispersion relation (Eq. (48)), the wavelength of waves which excites the vessel is decreased. By more frequency increment, this wavelength is further decreased so that the wavelength will be negligible compared to the length of vessel and can be considered as the water ripples. On this condition, the water ripples have a negligible effect on the vessel.

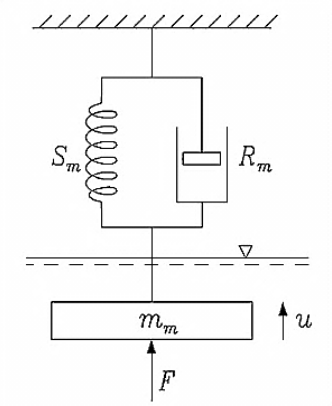

Fig. 16 A spring-damping mass systems with a underwater fluctuating mass

Therefore, the kinetic energy of the fluid particles around the vessel which are affected by its motion and velocity is also constant. However, given that in high frequencies, the vessel will fluctuate in very small periods, the water trapped between two demi-bodies will be less excited. By more frequency increment, the water particles will have constant fluctuations and therefore, the potential energy of the waves crest and trough will tend to become a constant value. On the other hand, the dominant damping is caused by the energy of waves which is generated by the vessel. In high frequencies the vessel will excite the fluid around itself at lower amounts. Therefore the damping tends to become a constant value too.

7. Conclusion

As mentioned before, motions and high accelerations in vessels (especially in high-speed vessels) have a negative effect on vessel operation, crews, passengers and equipment's. Therefore, control systems are used in order to control these motions and accelerations and diminish these unpleasant motions. In this regard, one of the most commonly used controlling elements is foil which is installed between the two bodies of the vessel and by changing its attack angles; it can affect and control the motions of the vessel. A question that arises in this regard and has not yet been answered is the effect of foil on motion equations coefficients of these vessels. In order to answer this question, there are two approaches: experimental and numerical. In the past, experimental methods to investigate the hydrodynamics of vessels were the popular methods due to lack of computer hardware. Experimental methods are usually expensive and require meticulous laboratory equipment. With the advance of science in the field of computer hardware, the feasibility of using a computer to study the vessel hydrodynamics has been provided. Governing equations of a rigid body dynamics together with CFD finite volume method governing equations can be solved using computers and CFD. The main conclusions of this study are as follows:

1) Applying the CFD finite volume numerical method to determine the hydrodynamic coefficients of high-speed vessels, which solves the RANS and Mass conservation equation, is a very efficient and accurate method spending less time and money, and allowing investigation of the effects of various parameters on the hydrodynamic coefficients of vessels.
2) Added mass and damping hydrodynamic coefficients of catamaran with and without the foil are independent of the frequency at high frequencies.
3) The foil effects on the added mass coefficients are negligible at all frequencies. Also, their effect on damping coefficients at high frequencies (which corresponds to high-speeds) is almost negligible.
4) The location of foil along longitudinal direction of the hull did not affect a lot to the added mass coefficients.
5) It was demonstrated that the negative added mass spreads in frequency domain considerably wide in the case of without foil.

REFERENCES

[1] Troesch, A. W.: On the hydrodynamics of vertically oscillating planing hulls, Journal of Ship Research, Vol. 36, No.4, pp. 317-331, Dec. (1992)

[2] Ursell, F, (1949). On the heaving motion of a circular cylinder on the surface of a fluid. Quart. J. Mech. Appl. Math., 2:218–231. https://doi.org/10.1093/qjmam/2.2.218.

[3] Tasai, F. (1960). Measurement of the wave height produced by the forced heaving of cylinders, Reports of Research Institute for Applied Mechanics , 8:279–310. https://doi.org/10.2534/jjasnaoe1952.1960.107_33.

[4] Porter, W. R. (1960). Pressure distributions added mass and damping coefficients for cylinders oscillating in a Free Surface, PhD thesis, University of California, Inst. of Eng. Research, Berkeley.

[5] . Paulling, J. R. and Richardson, R. (1962). Measurement of pressure, forces and radiating waves for cylinders oscillating on a free surface, Technical report, University of California, Inst. of Eng. Research, Berkeley.

[6] Fridsma, G.: A systematic study of rough-water performance of planing boats, Davidson Laboratory, Report No. 1275, Stevens Institute of Technology, Hoboken, N.J, (1969)

[7] Fridsma, G.: A systematic study of rough-water performance of planing boats (irregular waves-parts 2), Davidson Laboratory, Report No. DL-71-1495, Stevens Institute of Technology, Hoboken, N.J, (1971)

[8] Ogilive, T. F., Shen, Y-T.: Flutter-like oscillations of a planing plate, Department of Naval Architecture and Marine Engineering, Report No. 146, The University of Michigan, Ann Arbor. (1973)

[9] De Zwaan, A.P.: Oscillation eproeven met een planerendo wig. Report No. 376.M, Baboratorium voor scheepsbouwkunde, Technische Hogeschool, Delf, The Netherland, (1973)

[10] Martin, M.: Theoretical determination of porpoising instability of high-speed planing boats, Journal of Ship Research, 22, 1, March (1978)

[11] Martin, M.: Theoretical prediction of motions of high-speed planing boats in waves, Journal of Ship Research, 22, 3, Sept (1978)

[12] Payne, P. R.: Boat 3D- a time-domain computer program for planing craft, Payne Associates, Stenensville, Md, (1990)

[13] Insel, M., Molland, A., 1992. Investigation into the Resistance Components of High Speed Displacement Catamarans, Transactions of Royal Institute of Naval Architects, pp. 1–20.

[14] . G. J. Grigoropoulos, et al.: Transient waves for ship and floating structure testing, Elsevier Science, (1994).

[15] Stephen, M., Klaka K.: Investigation into Wave Loads and Catamarans, Hydrodynamics of High-speed Craft Conference (RINA), 24-25 November 1999, London, UK, (1999).

[16] Varyani, K.S., Gitiganti, R.M., and Gerigk, M. (2000). "Motion and Slamming Impact on Catamaran", Ocean engimeering, Vol. 27, pp729-744.

[17] Chen, H. C., Liu, T., Huang, E. T.: Time-domain simulation of large amplitude ship roll motions by a chimera RANS method, Proceedings, 11th International Offshore and Polar Engineering Conference, June 17–22, Stavanger, Norway, vol. 3, 299–306. (2001)

[18] Miller, R., Gorski, J., Fry, D.: Viscous roll prediction of a cylinder with bilge keels, Proceedings, 24th Symposium on Naval Hydrodynamics, July, Fukuoka, Japan, (2002).

[19] Sato, Y., Miyata, H., Sato, T.: CFD simulation of 3-dimensional motion of a ship in waves: application to an advancing ship in regular head waves", Marine Science and Technology, 4, 108–116. (1999)

[20] Paterson, E. G., Wilson, R. V., and Stern, F.: General Purpose Parallel Unsteady RANS Ship Hydrodynamics Code: CFDSHIP-IOWA, IIHR Report 432, Iowa Institute of Hydraulic Research, University of Iowa, Iowa City, IA, November. (2003)

[21] . Rhee, S., Stern, F.: Unsteady RANS method for surface ship boundary layer and wake and wave field, International Journal of Num. Meth. Fluids, 37, 445–478. (2001). https://doi.org/10.1002/fld.183.

[22] Stern, F., Wilson, R. V., Colman, H., Paterson, E.: Comprehensive approach to verification and validation of CFD simulations— part 1: methodology and procedures, ASME Journal of Fluids Engineering, 123, 793–802. (2001). https://doi.org/10.1115/1.1412235.

[23] Lugni, C., Colagrossi, A., Landrini, M., Faltinsen, O.M., 2004. Experimental and numerical study of semi-displacement mono-hull and catamaran in calm water and incident waves. In: Proceedings of the 25th ONR Symposium on Naval Hydrodynamics. Canada.

[24] Weymouth, G. D, Wilson, R. V, Stern, F.: RANS Computational Fluid Dynamics Predictions of Pitch and Heave Ship Motions in Head Seas, Journal of Ship Research, Vol. 49, No. 2, pp. 80–97, June (2005)

[25] Souto-Iglesias, A., Zamora-Rodríguez, R., Fernández-Gutiérrez, D., Pérez-Rojas, L., 2007. Analysis of the wave system of a catamaran for cfd validation. Experiments in Fluids 42, 321–333. https://doi.org/10.1007/s00348-006-0244-4.

[26] Larsson, L., Stern, F., and Visonneau, M.: Gothenburg 2010, A Workshop on Numerical Ship hdrodynamics, (2010)

[27] Zaghi, S., Broglia, R., Di Mascio, A., 2011. Analysis of the interference effects for high-speed catamarans by model tests and numerical simulations. Ocean Engineering 38 (17–18), 2110–2122. (December 2011). https://doi.org/10.1016/j.oceaneng.2011.09.037.

[28] Hosseini., S. H. S.: CFD prediction of ship capsize: parametric rolling, broaching, surf-riding, and periodic motions, Ph.D, Mechanical Engineering, University of Iowa, (2009).

[29] Journee, J. M. J.: Experiments and Calculations on Four Wigley Hull forms, Delft University of Technology, Ship Hydrodynamic Laboratory, Report No. 909, February. (1992)

[30] Karafiath, S., Fisher, C.: The effect of Stern Wedges on Ship Powering Performance, Naval Engineers Journal, May, (1987).

[31] Tsai, J.F., Hwang, J.L., Chau, S.W., and Chou, S.K.: Study of Hydrofoil Assistance Arrangement for Catamaran with Stern Flap and Interceptor, FAST 2001, Southampton, UK, Sep., (2001)

[32] . Steen, S., Alterskjar, S, A., Velgaard. A., Ingebjorn A.: Performance of a planing craft with mid-mounted interceptor, Fast 2009, Greece, October (2009).

[33] Menter, F., Kuntz, R. M., and Langtry, R.: Ten Years of Industrial Experience with the SST Turbulence Model, Turbulence, Heat and Mass Transfer, (2003)

[34] . Falnes, Ocean Waves and Oscillating Systems, Cambridge University Press, 2004.

[35] . O.M.Faltinsen, Sea Loads on Ships and Offshore Structures, Cambridge University Press, 1998.

Submitted: 20.05.2015.

Accepted: 23.01.2016.

Amin Najafi, najafi.sharif@yahoo.com, Mohammad Saeed Seif
Center of Excellence in Hydrodynamics and Dynamics of Marine Vehicles, Mechanical Engineering Department, Sharif University of Technology, Azadi Ave., Tehran, Iran